Intermetallics 159 (2023) 107932

Contents lists available at ScienceDirect

Intermetallics

journal homepage: www.elsevier.com/locate/intermet

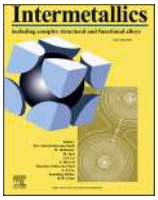

Acoustic emission and DSC investigations of anomalous stress-stain curves and burst like shape recovery of $Ni_{49}Fe_{18}Ga_{27}Co_6$ shape memory single crystals

Sarah M. Kamel [a,b], Lajos Daróczi [a], László Z. Tóth [a], Elena Panchenko [c], Yuriy I. Chumljakov [c], Nora M. Samy [a,b,d], Dezső L. Beke [a,*]

[a] Department of Solid State Physics, Doctoral School of Physics, Faculty of Science and Technology, University of Debrecen, P. O. Box 400, H-4002, Debrecen, Hungary
[b] Physics Department, Faculty of Science Ain Shams University, Abbassia, 11566, Cairo, Egypt
[c] Siberian Physical Technical Institute, Tomsk State University, 634050, Tomsk, Russia
[d] Department of Physics, Faculty of Education, Ain Shams University, Roxy, 11341, Cairo, Egypt

ARTICLE INFO

Keywords:
Shape-memory alloy
Martensitic transformation
Shape-memory effect
Martensitic structure
Differential scanning calorimetry
Acoustic emission spectroscopy

ABSTRACT

Simultaneous acoustic emission, AE, and DSC measurements under compression along $[110]_A$ direction were carried out on $Ni_{49}Fe_{18}Ga_{27}Co_6$ shape memory single crystals. The compression resulted in anomalous stress-strain loops with stress drops/jumps on it, reflecting a sudden formation/dissolution of a more stable (detwinned) martensite structural modification than the thermally induced (twinned) one. The final detwinned martensite, obtained below a certain temperature, was stable even after downloading: during heating it showed a burst-like recovery at about 35K higher transformation temperature than that of the thermally induced one, with an audible click. It was obtained that the number of acoustic events showed strong asymmetry: e.g. for stress induced transformations the number of hits for uploading was larger. Simultaneous measurements of stress-time curves and AE versus time revealed that in the nucleation/dissolution processes in both (up and down) directions, as an intermediate step, the twinned martensite was first formed and resulted in additional AE events. This was interpreted by the easy as well as difficult nucleation of the twinned and detwinned martensites, respectively. The stress drops on the uploading stress-strain curve were attributed to subsequent nucleation of the detwinned martensite from the twinned modification and were followed by a sharp decrease of the AE activity. This indicated that the formation of detwinned martensite is a sudden, fast process and can take place without significant elastic energy storage. This was also in agreement with the fact that during burst like thermal recovery the width of the transition was very small ($A_f \cong A_s$). Similarly, during downloading the stress jumps were interpreted as sudden dissolutions of the detwinned phase by retwinning and at all stress jumps there were local maxima on the AE activity curve.

1. Introduction

During forward (cooling) or reverse (heating) martensitic transformations the transition between the austenite and martensite typically takes place slowly in a sense that on a DSC curve, taken e.g. at 10K/min rate, the peak of transition is about 10–50 K wide, i.e. the duration of the transition is in the order of minutes. However, there are observations, when this duration is orders of magnitude shorter: it occurs in a very narrow temperature interval less than 10^{-3}K [1–8]. This fast transition is often accompanied with jumping of the sample and with an audible click, and is called burst-like transition. It is worth to make distinction between burst-type transition during forward transformation [1] or during heating [2–8]. This latter type can also be referred in shape memory alloys as "burst-like strain recovery" [2–5]: in this case it can happen that, after stress induced martensite transformation, the sample turns back to its original shape only during heating. This phenomenon evoked increasing interest in recent years [2–11]. The DSC peak belonging to this transformation back to the austenite is at considerably higher temperature than the heating peak, obtained during the usual thermally induced transformation without martensite stabilization [2,

* Corresponding author.
E-mail address: dbeke@delfin.unideb.hu (D.L. Beke).

https://doi.org/10.1016/j.intermet.2023.107932
Received 9 January 2023; Received in revised form 18 April 2023; Accepted 22 April 2023
Available online 28 April 2023

9].

The bust-like strain recovery can be typically achieved by loading under uniaxial stress at a fixed temperature. Fig. 1 illustrates this schematically. In Fig. 1a the normal stress induced transformation from austenite to martensite and back is shown ($T > T_c$, where T_c is a critical temperature, close to the austenite finish temperature, A_f, [9], above which the stress-strain curve is a closed loop). Here the overall slope of the uploading branch is positive. Fig. 1b shows an anomalous $\sigma\sim\varepsilon$ curve still for $T > T_c$, but there are stress drops/jumps both on the up and down branches and the overall slope is negative for the uploading branch. Fig. 1c shows the $\sigma\sim\varepsilon$ curve at $T < T_c$: in this case, the uploading curve is similar to the curve shown in Fig. 1b and after removing the stress, there is a residual strain corresponding to the stabilized martensite. After c) anomalous stress-strain loading a burst-like strain recovery can be observed.

Both the martensite stabilization, and the anomalous stress-strain curves, are interpreted by the presence/competition of two different martensitic structural modifications. In $Ni_{49}Fe_{18}Ga_{27}Co_6$ single crystal these were identified as twinned 14 M martensite, as well as $L1_o$ detwinned tetragonal martensite, respectively [3,9], and the detwinning as well as retwinning of these was important in the stabilization. In other shape memory alloys, showing the above martensite stabilization, there is a similar competition between two martensite modifications. In Cu-based alloys the β' (18R monoclinic) and/or twinned γ' (2H orthorhombic) martensites as well as detwinned γ' phases, respectively take place in the process [7,8,12], while it was found in polycrystalline NiTi alloy [13] that the reorientation of the martensite was responsible for the stabilization.

In $Ni_{49}Fe_{18}Ga_{27}Co_6$ single crystals the twinned martensite, *TM*, can be produced by usual thermally induced transformation, while the detwinned martensite, *DM*, typically can be formed during stress induced martensitic transformation [2,3,9]. The martensite stabilization, related to the dominant formation of the detwinned structural modification can be explained by difficulties in the formation of the habit plane between austenite and detwinned martensite [9,14,15]. In addition, during burst-like thermal recovery, a large overheating is requested and the burst-like transition occurs at a temperature, high enough to start the transformation. According to Refs. [2,3], formation of dislocations hindering the formation of the *DM/A* interphase boundaries or/and difficulty in retwinning of the detwinned martensite [14] can also play a role in such overheating. In a very recent paper [11] a thermodynamic description of the anomalous stress-strain curves was given and it was shown that a stress drop, $\Delta\sigma$, on the uploading branch can appear if the *TM* nucleates first (i.e. if the martensite start stress is larger for D*M*: $\sigma_{DM} > \sigma_{TM}$), and at a certain martensite volume fraction, ξ_c, *DM* nucleates:

$$\Delta\sigma = -\left(\varepsilon^{trDM} - \varepsilon^{trTM}\right) S(\xi_c)\xi_c. \quad (1)$$

Here ε^{trDM} and ε^{trTM} are the transformation strains and S(ξ) is the effective stiffness of the $TM + A$ two-phase system [11]. The stress drop is negative if $\varepsilon^{trDM} > \varepsilon^{trTM}$ and $\sigma_{DM} > \sigma_{TM}$ first of all because the nucleation energy of *DM* is larger than for *TM*. After the stress drop the process can be repeated and two scenarios are possible: i) for large stress drop the system falls to the elastic regime, and the further growth starts with the slope $S(\xi_c)$, or ii) for moderate stress drop the *TM* martensite continues its growth.

It is also often observed that the transformation is not complete, i. e. it represents only a certain fraction of the whole transformation [1,7–9], but there are examples when it was complete i.e. the whole sample has been transformed during a burst-like strain recovery [4,10]. Furthermore, it was also observed that these properties are strongly anisotropic and can differ considerably along different crystallographic orientations [2]. Indeed it was observed for instance in Fig. 1 of [2] (see Fig. 1 therein) that the upper branch of the $\sigma\sim\varepsilon$ curves, along $[100]_A$ as well as $[110]_A$ directions in a $Ni_{49}Fe_{18}Ga_{27}Co_6$ single crystal was normal as well as anomalous, respectively. Similar anisotropy of transformation characteristics were documented already in 1999 in Cu-based shape memory alloys [16].

Thus, investigations on the thermal recovery behaviour and on shapes of the $\sigma\sim\varepsilon$ curves were carried out recently on $Ni_{49}Fe_{18}Ga_{27}Co_6$ [2] and $Ni_{51.1}Fe_{16.4}Ga_{26.3}Co_{6.2}$ single crystals [9]. Such types of ferromagnetic alloys represent promising materials with magnetic field induced strain, similar to the classical Ni_2MnGa alloys. In addition, while the latter one is brittle, the $Ni_{49}Fe_{18}Ga_{27}Co_6$ alloys are much more ductile [17]. Furthermore, these alloys have good reproducibility during superelastic cycling, which is an advantage in elastocaloric or magnetocaloric applications [18,19]. Since the stress induced martensite stabilization can have an influence on the cycling actuation behaviour [9], further works are desired for better understanding of these processes.

In this communication we report results on experimental investigation of anomalous stress-strain curves taken at different temperatures and on the burst-like recovery in $Ni_{49}Fe_{18}Ga_{27}Co_6$ (at%) single crystals. The most important novelty is the measurements of acoustic emission signals during the above processes: the accompanied audible click is a robust indication of acoustic activity, and investigations of the details can bring new information for better understanding.

2. Experiments

The $Ni_{49}Fe_{18}Ga_{27}Co_6$ (at%) alloy was prepared using vacuum induction melting. The single crystals were grown by Bridgman method in helium atmosphere at Tomsk University, Russia. The as-grown sample had rectangular shape with dimension 3.5 mm × 3.6 mm × 4.7 mm. From this a smaller piece (with dimensions of 1 mm × 1.5 mm × 2 mm) was cut out using an spark erosion machine (sample A) and annealed at 1473 K for 1h in argon atmosphere, which is well above the order-disorder transition temperature ($T \cong 975\,K$ [20,21]), and then water quenched. The B_2 high temperature phase of the quenched crystals

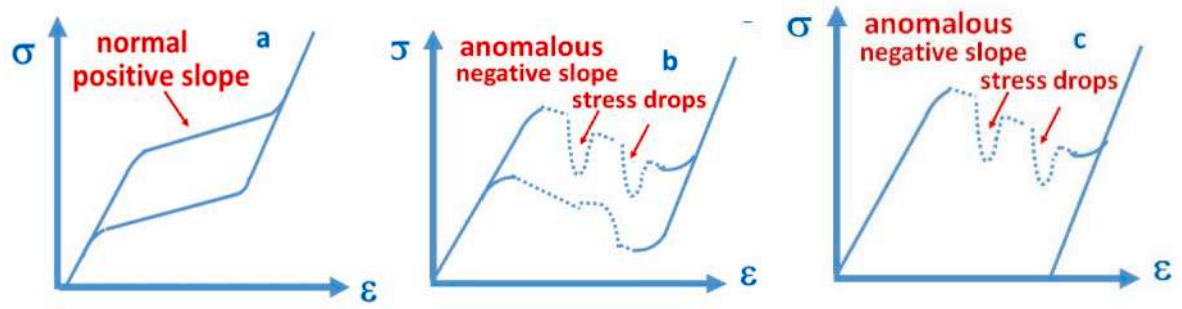

Fig. 1. Stress versus strain curves at fixed temperature schematically (see also [11]: a) shows a normal behaviour with a positive slope of the uploading branch, while b) illustrates the anomalous behaviour: the overall slope is negative and there are stress drops on it. c) shows the anomalous behaviour with a residual strain (stabilized martensite has been formed).

undergoes to a martensitic transformation to the $L1_0$-martensite. According to the results of TEM investigations [20,21] the above homogenization and quenching resulted, immediately after quenching, in the presence of γ -phase precipitates with a size of 5–15 μm (see also [22]).

Samples of disk as well as rectangular shape were also cut, from the same as grown piece and annealed at 1473 K for 1h in argon atmosphere and then quenched (samples B and C, respectively). Sample B was used, just after quenching, for DSC and acoustic emission, AE, measurements. Furthermore, the rectangular shaped sample C was used for DSC and compression measurements. Table 1 summarizes the information on samples.

The calorimetric measurements and their evaluations were carried out, similar to the usual procedure described in Refs. [23–26]. For The DSC measurements a PerkinElmer DSC7 device (PerkinElmer Inc., Waltham, MA, USA) was used with 10K/min scanning rate. The calibration was made with the melting point of the pure Indium and Tin.

The acoustic emission, AE, measurements were carried out in a modified DSC device, enabling simultaneous DSC and AE measurements [23,26]. For AE measurements the Sensophone AED404 Acoustic Emission Diagnostic Equipment (Geréb and Co.,Ltd.,Budapest, Hungary) with piezoelectric sensor (MICRO-100S from Physical Acoustic Corporation, Princeton junction, NJ, USA) was used. The microphone had a good frequency response between 100 KHz and 1 MHz, which is nearly flat in the range between 0.2 and 1 MHz (at about ~ 75 dB in average) with maximum ± 10 dB deviation (1V reference value). The sensor was coupled to the sample via 18 mm long steel waveguide (with 1 mm large diameter), in order to provide thermal isolation from the sample when its temperature was widely varied. Two methods of data acquisition were used: "streaming mode" (continuous acquisition of row signals with a maximum 8 MS/s sampling rate) or "hit" mode" (collection of signals above a fixed threshold level, using an analog-digital converter). The analog-to-digital converter sampling rate was 16 MHz, and the setup had a band-pass from 30 KHz to 1 MHz. A 30 dB preamplifier, and a main amplifier (logarithmic gain) with 90 dB dynamic range were used. The threshold level was determined from measurements carried out in austenitic state for cooling and martensitic state for heating, respectively. The amplitude, A, area, S, and energy, E, of acoustic avalanches were calculated from the detected voltage, U(t) (temporal avalanche shape) according to their usual definitions [23,26]: A is the maximum value, $S = \int_0^D U(t)dt$, and $E = \frac{1}{R}\int_0^D U^2(t)dt$, where R is an arbitrarily chosen resistance (R = 1MΩ) and D is the duration time of the avalanche.

The compression measurements were carried out using Instron testing machine (No. 4465) at strain rates 0.002–0.003s^{-1}. In this case the AE sensor (enabling detection of AE signals during the compression test) was fixed to the top steel pushing head.

3. Results

3.1. Thermally induced martensitic transformations

The results of the DSC measurements for heating and cooling, with 10K/min rate, are shown in Fig. 2a, 2b and 2c for samples A, B and C, respectively.

All investigated samples had similar heat and entropy of transformation (the experimental error bars are ±3% and ±5%, respectively), while there is a shift in the transformation temperatures and widening of the transformation interval for samples used just after quenching. The detailed results are shown in Table 2.

The measured acoustic signals (hit mode, at 10K/min rate), as an illustration, are shown for sample *B* in Fig. 3. The cumulative energy was calculated from the acoustic energies of avalanches, E_i, as $E_\Sigma = \Sigma E_i$ and the AE activity ($\frac{dN}{dt}$, where N is the number of hits) is also shown. The correlation between the $\frac{dN}{dt}$ and E_Σ curves can be seen: each jump in E_Σ corresponds to increased activity.

Fig. 4 shows the hysteresis loops of the martensitic transformation as constructed from the measured DSC curves [6] for A, B and C samples (4a, 4b and 4c, respectively). The martensite volume fraction was calculated using the normalized partial integral of the Q/T curves (Q is the heat of transformation and T is the temperature), and the value of the entropy, used for normalization, was determined from the measured DSC according to the usual procedure [25] (see also Table 2). The areas of the hysteresis curves provide the dissipative energies per cycle as 11.8, 2.0 and 7.0 J/mol for samples A, B and C, respectively.

Fig. 5 shows, as an illustration, the energy distribution functions of AE signals during heating and cooling for sample *A*. The AE measurements were repeated 12 times and exponents were the same within the error bars. Table 3 shows the values of the exponents of the distributions of energy and the maximum amplitude, A, for thermally induced transformations in samples *A* and *B,* together with the energy exponent for burst-like recovery (see also below). The probability distribution functions of a measured parameter, x, for intermittent processes with avalanches (driven criticality [26–28]) can be described by a truncated power law as

$$P(x) = C\, x^{-\tau}\, exp\left(-\frac{x}{x_c}\right) \tag{2}$$

where τ is the characteristic exponent, x_c is the cutoff value and C is a normalization factor. It can be seen that indeed the plots on Fig. 5 can be well approximated by straight lines over two-three orders of magnitude on the energy scale, i.e., we can take $\exp(-x/x_c) \cong 1$ in Equation (2). In order to get the exponents from Equation (2), the PDF functions (calculated using logarithmic boxing of the quantities $P(E_i) \sim \frac{N_i}{N}$, where N_i and N denote the number of events at a certain value of E_i and the number of all hits, respectively) were fitted using a two parametrical nonlinear fitting by the Levenberg-Marquardt least squares method.

In addition, in accordance with the well-known power-type scaling rules [27–30], relations between measured AE parameters (e.g. $E \sim A^\chi$, and $S \sim A^\delta$ where χ and δ are the characteristic exponents) were also investigated. As an illustration Fig. 6 shows the *logE* versus *logA* functions for one run measured on sample *B,* in heating and cooling, respectively. These results are published in a separate paper on these scaling rules [30] and thus will not be detailed here.

3.2. Results obtained during compression along the [110] axis and AE as well as DSC results obtained during burst-like shape thermal recovery

Fig. 7a shows the stress-strain curve for sample A. The sample was compressed at 283 K ($> A_f$) along the $[110]_A$ axis. It was also repeated at 293 K (Fig. 7b) and a similar stress-strain curve was observed. It can be seen that the curves are anomalous in that sense that instead having a plateau with small positive slope, they have overall negative slope with two stress drops on it. Furthermore, after removing the stress, the sample remained in the martensitic state and did not transform back to austenite, with a residual strain 6%. This indicates that a stabilized martensite has been formed finally since the thermally induced martensite is not stable at 283 K (see also Table 2).

Table 1
Information on samples used.

Sample	shape	Size (mm)	Mass (mg)	Heat treatments
A	rectangular	1 × 1.5 × 2	16	1h at 1473 K in argon atm., quenched + kept at room temperature for 3 months
B	disk	diameter: 3 thickness: 0.2	16	1h at 1473 K in argon atm., quenched
C	rectangular	1.9x2.2x 1.3 (DSC)	49	1h at 1473 K in argon atm., quenched
		1.9x2.2x3.0 (stress-strain)	104	

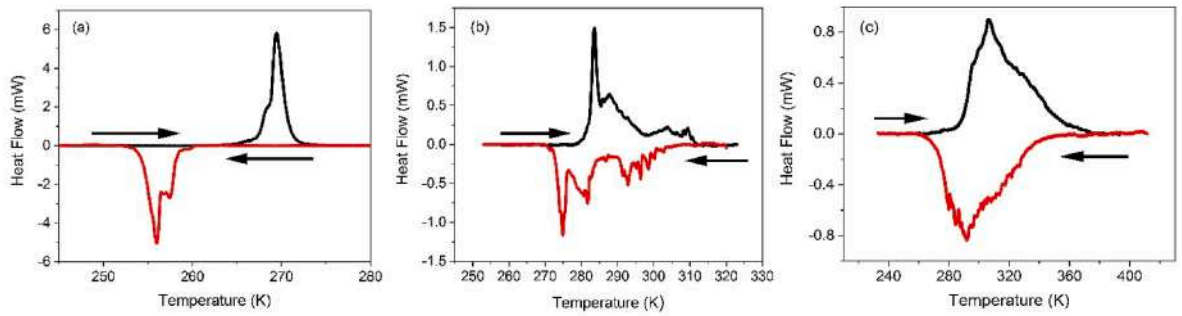

Fig. 2. DSC peaks during heating (black lines) and cooling (red lines) for sample *A* (a), *B* (b) and C (c), respectively (10K/min rate).

Table 2
Heat and entropy of transformation (Q and S, respectively) for heating, h, and cooling, c, obtained in samples A, B and C.

No.	Rate = 10K/min	M_s	M_f	Q_c	S_c	A_s	A_f	Q_h	S_h
		K	K	J/mol	J/mol K	K	K	J/mol	J/mol K
A		260	252	−257	-1.00	264	273	256	0.95
B		305	272	−250	-0.90	280	312	256	0.90
C		350	268	−240	-0.80	267	367	248	0.80

Fig. 8a shows the DSC results for heating up of the compressed sample after compression at 283 K. Two peaks were observed. The second peak during the first run represents the burst transition of the sample from martensite to austenite, in which the transformation temperature is shifted to a higher temperature by 35K. The sample had recovered fully after this peak, during this transformation and an audible click was heard. There is also a smaller peak at lower temperature (only by about 10K higher than the temperature of the martensite to austenite transformation temperature during thermally induced transformations). Interestingly, after the compression at 293 K only one DSC peak was observed (Fig. 8b) at temperature close to the temperature of the second peak in Fig. 8a. Since during bust-like transitions (2nd peak in Fig. 8a and the peak on Fig. 8b) the sample jumped, we made efforts to fix the sample (by silicon grease) in order to ensure the heat contact as good as possible. This attempt was less successful for sample compressed at 283 K (at second peak in Fig. 8a), where we had a problem of a sudden change of the base line, thus the area of the second peak is probably not realistic in Table, 4 and the corresponding values of Q and S have a question mark, indicating this.

The summary of DSC results obtained on sample A during thermally induced transformation and during the first run for heating after compression at 283 K and 293 K can be found in Table 4. The units of the heats and entropies of transformations here (in contrast to data given in Table 2) are given in units *J* as well as *J/K* and thus denoted by *q* and *s*, respectively. T_{ph} and T_{pc} are the peak positions for heating and cooling,

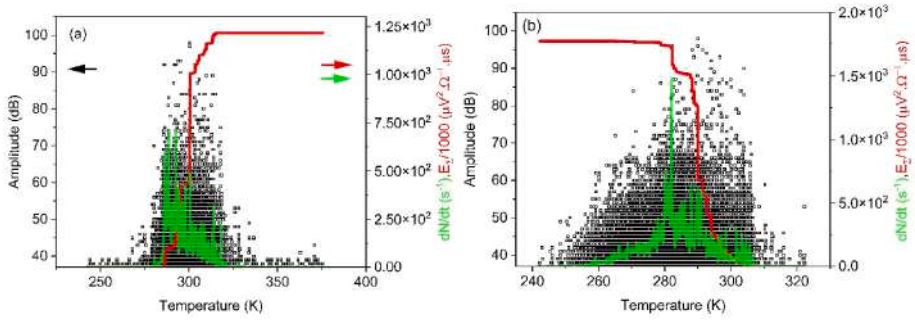

Fig. 3. Acoustic signals during heating (a) and cooling (b) for sample *B* (hit mode). Squares correspond to amplitudes of hits and the continuous red and green lines show the temperature dependence of the cumulative energy ($E_\Sigma = \Sigma E_i$), as well as the acoustic activity, respectively (their corresponding numbers and units are given on the right vertical axis: the numerical values of E_Σ are the same as those for $\frac{dN}{dt}$, after dividing by 1000).

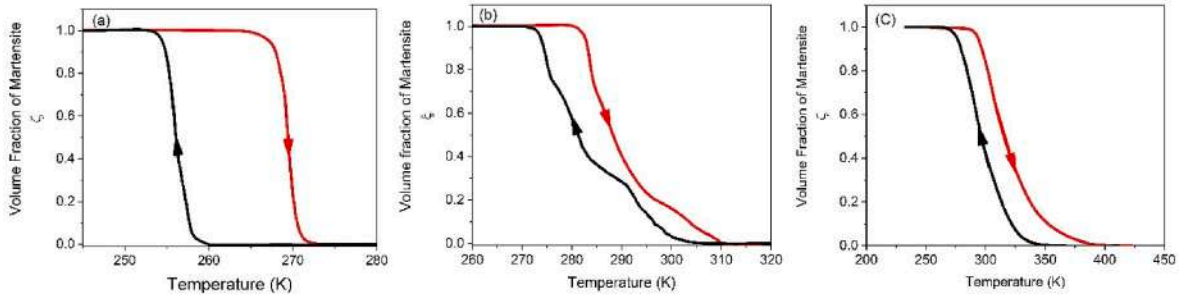

Fig. 4. Thermal hysteresis loops for samples *A* (a), B (b) and *C* (c), respectively.

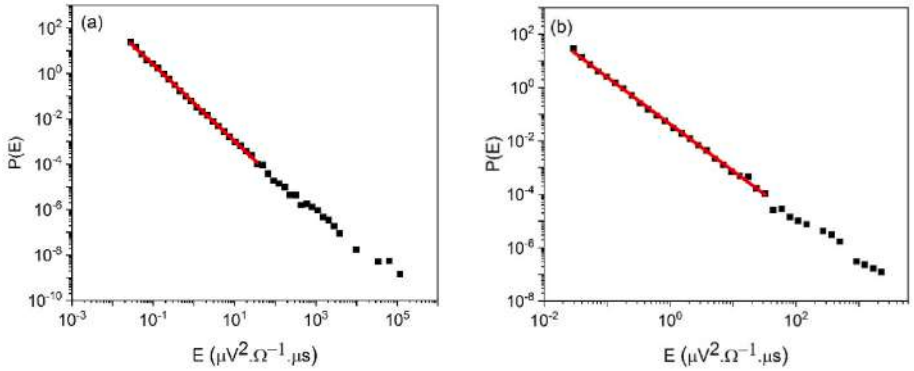

Fig. 5. Energy distribution functions; Log P versus log E, obtained from acoustic measurements during heating (a) and cooling (b) of sample A.

Table 3
Energy and amplitude exponents (ε and α, respectively) as well the number of hits (N) and the total energy (E_t). The error bars for the amplitude and energy exponents are about ±0.3 and ± 0.1, respectively.

Sample	AE for Heating				AE for Cooling			
	N	α	ε	E_t	N	α	ε	E_t
A	18325	2.4	1.7	$8.18x10^3$	11623	2.7	1.7	$4.34x\ 10^3$
A (Burst)	2823	3 .0	1.9	$1.56x10^3$	–	–	–	
B	31738	2.5	1.6	$4.76x\ 10^4$	47834	2.6	1.6	$6.39\ x10^4$

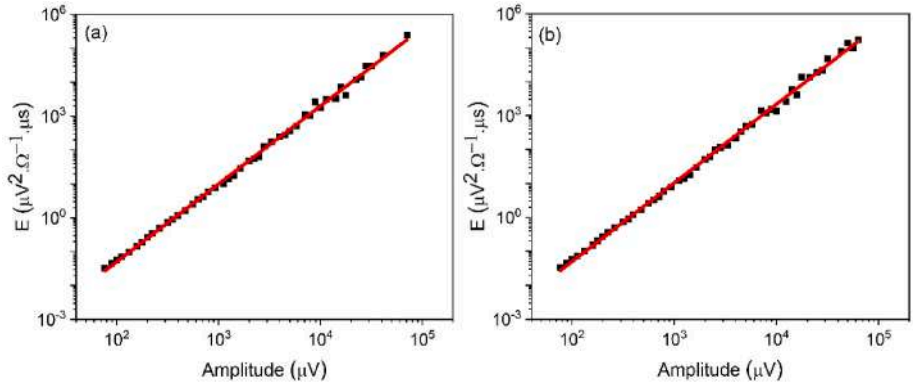

Fig. 6. Illustration of the scaling rule between the energy and the peak amplitude for martensitic transformation in sample B, for heating (a) and cooling (b), respectively. The power exponents are the same, $\chi = 2.3$, for heating and cooling. Similarly, the values of δ were also the same: $\delta = 1.4$.

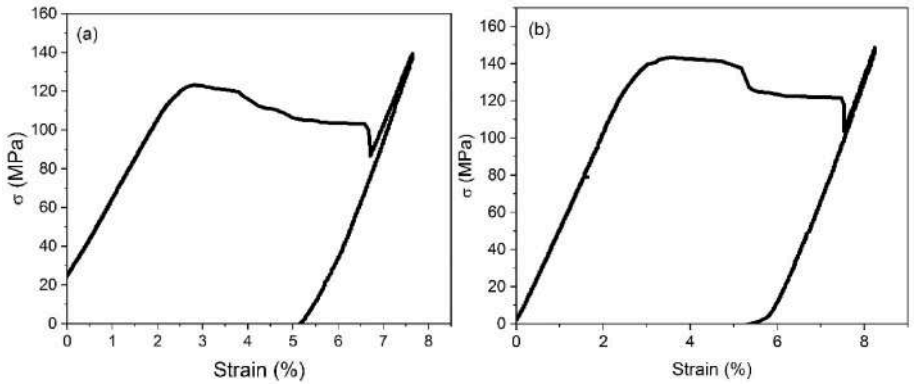

Fig. 7. Stress-strain curve along $[110]_A$ direction for sample A: (a) at 283K, (b) at 293K, taken with $0.003s^{-1}$ strain rate.

respectively and e.g. $T_{pc} = \frac{M_s+M_f}{2}$. After compression there are two peaks (see also Fig. 8a) for heating and no peak for cooling during the first run at 293K.

Fig. 9 shows the acoustic signals collected during bust-like shape recovery (hit mode). Points correspond to amplitude of hits and the continuous lines show the temperature dependence of acoustic activity

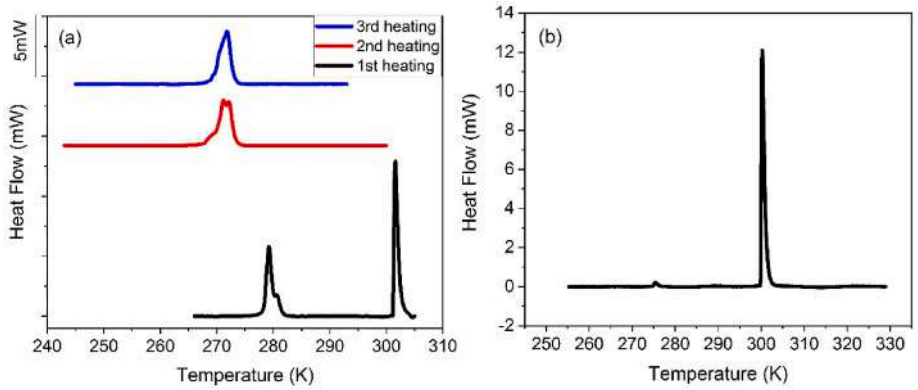

Fig. 8. a) DSC curves for the first run after the compression along the [110] direction at 283 K, as well as after the second (fully thermally induced) run (sample A). b) DSC results obtained during shape recovery after compression at 293 K (see also Table 4).

Table 4
Summary of DSC results obtained on sample A during thermally induced transformation and during the first run for heating after compression at 283 K and 293 K.

transitions	q_c (J)	q_h (J)		s_c (J/K)	s_h (J/K)		T_{pc} (K)	T_{ph} (K)	
thermally induced without compression	−0.0673	0.0670		−0.000261	0.000248		256	269	
thermally induced (burst-like) after compression at 283 K	–	*h1*	*h2*	–	*h1*	*h2*	-	*h1*	*h2*
		0.0530	0.0674?		0.000190	0.000223?		279	302
thermally induced (burst-like) after compression at 293 K	–	–	0.0615	–	–	0.000205	–	–	300

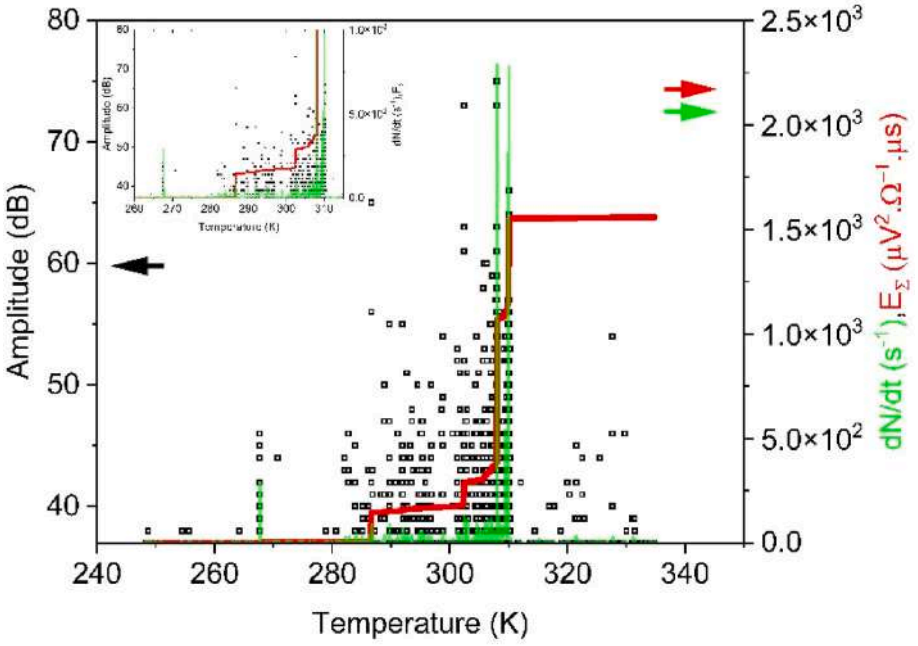

Fig. 9. Acoustic signals (squares), acoustic activity (green curve) and the cumulative energy (E_Σ, read curve) during burst-like shape recovery: sample A, after compression at 283 K. The numerical values for the activity and cumulative energy in the given units on the right-hand vertical axis are the same, i.e. the scales are identical.

as well as the cumulative number of energy. It can be seen that the peaks of AE activity correlate very well with the sharp jumps on the E_Σ curve, which agree well with the DSC peak positions in Fig. 8a.

Fig. 10 shows the energy distribution function for the strain recovery process. The values of the amplitude and energy exponents are a bit larger for the burst-like recovery (see also Table 3) than for those belonging to thermally induced transformations.

3.3. Stress-strain curves during compression along the [110] axis at different temperatures

For these measurements, samples C with mass 104 mg were used (see also Table 1). The results on thermally induced DSC measurements are already shown in Fig. 2 and Table 2.

Stress-strain curves measured during compression along the [110] axis taken at different temperatures are shown in Fig. 11. It can be seen that for temperature above 383 K these are closed loops with a certain amount of hysteresis: the area of the loops has a moderate temperature

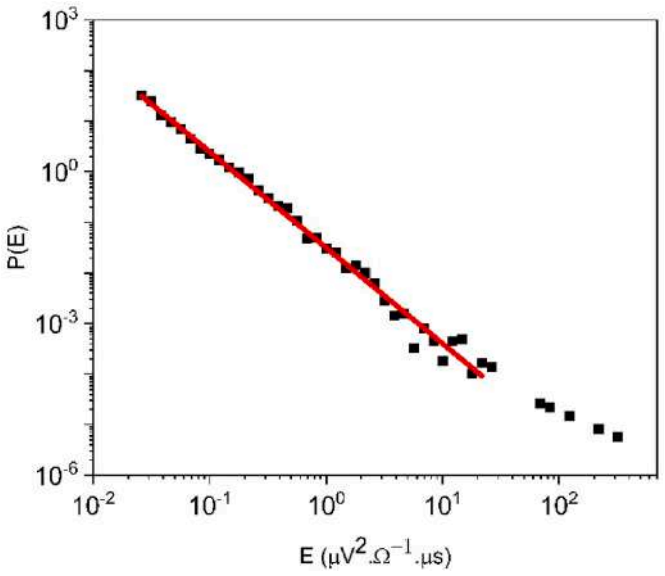

Fig. 10. Energy distribution function; Log P versus log E for burst-like the strain recovery process: sample A, first run after compression at 283 K.

dependence: the dissipative energy changes from 33J/mol (at 383 K) to 28J/mol (at 353K). Interesting feature is that the overall slope, similarly to the uploading branches in Fig. 7, is negative, in contrast with the usual superelastic stress-strain curves and this is in accordance with the results of [2,4,9]. In addition, there are stress drops as well as stress jumps on the uploading and downloading curves too, and during the largest stress jump usually an audible clicking noise was detected.

3.4. AE during compression along the [110] axis

Fig. 12 shows the acoustic signals (hit mode), the cumulated number of signals, the AE activity ($\frac{dN}{dt}$) as well as the stress versus time during uploading and downloading at 383 K. It can be seen that AE events are present already along the first, almost linear part of the uploading stress curve with high numbers at up to about the first stress drop and there are practically no signals after the second stress drop. Regarding the first part, the situation is similar for downloading: there are signals before the first stress jump. On the other hand, there are also AE events even during the last part, which has a similar slope as the first (austenitic) part of the uploading curve. The activity versus time curves, besides that they confirm the above conclusions, provide interesting additional information. For uploading the activity definitely increases up to reaching the first stress drop, then has a sudden drop at around it and shows a maximum at the second stress drop. Similarly, there is some activity before reaching the first stress jump for downloading and the maxima of the activity versus time curve correlates with the stress jumps. Finally, here there is a gradually decreasing activity during the last part.

Fig. 13 shows, as an illustration, the energy distribution functions of AE events; Log P versus log E, obtained from acoustic measurements during loading at 383 K (a) and the corresponding maximum likelihood fit (b). The likelihood fit is a recommended method to check the reliability of exponents calculated from the log P versus log E plots [31]. It can be seen that the position of the plateau on the ε versus log E plot corresponds very well to the value of ε obtained from the fit of Eqn. (2) as indicated in Fig. 13a.

It can be seen from Table 5, which contains the peak amplitude and energy exponents as well, that the values for uploading and downloading are the same within the error bars.

Fig. 14, as an illustration, shows the scaling relations between the AE parameters, E versus A as well as S versus A for uploading. It can be seen, that these, as expected, follow a power law behavior with exponents shown in Table 6. It can be seen that these exponents are the same, within the error bars, as the similar exponents obtained during thermally induced transformation (see the text below Fig. 6).

4. Discussion

4.1. Thermally induced transformations

As it can be seen from Figs. 3 and 5 as well as from Table 2 that the effect of the prehistory of samples is manifested in the change of the shift and width of the transformation as well as in the shape of the hysteresis loop. This can be attributed to the possible change in the size and

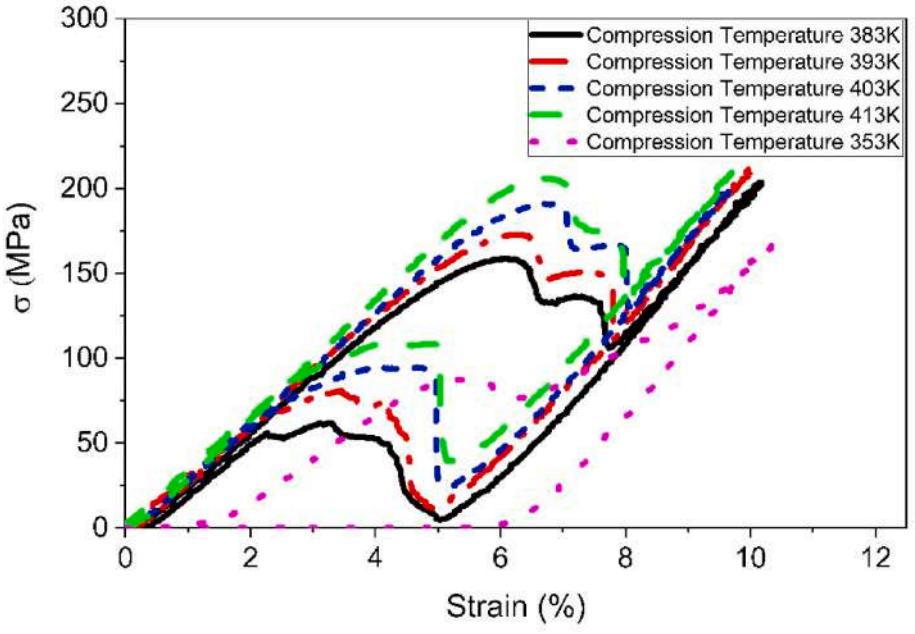

Fig. 11. Stress-strain curves during compression along the [110] axis: sample C at different temperatures. The curves were taken subsequently between 383K and 413 K, starting at 383 K, while the curve at 353K was taken after the above runs.

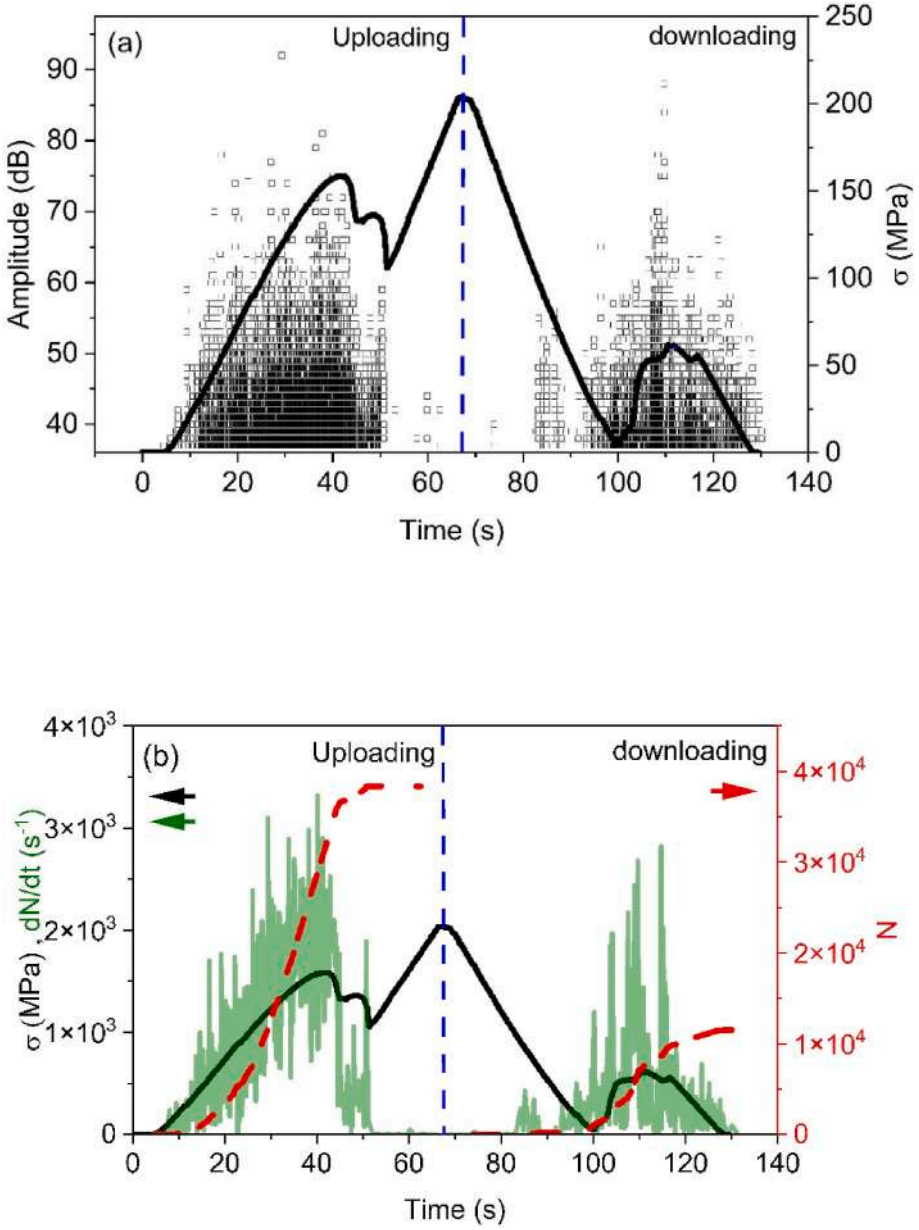

Fig. 12. Acoustic signals and the stress versus time curves for sample C: (a) during uploading and unloading. b) shows the cumulated number of signals (dashed red lines), the AE activity ($\frac{dN}{dt}$) (in green) as well as the stress curves (in black) for uploading and unloading at 383 K (the maximum of the stress curve corresponds to 200 MPa, in accordance with a)).

distribution of γ-phase precipitates [21–23]. On the other hand, the heats and entropies of transformations did not change considerably: they differ by a bit larger value than the error bar for sample C as compared to samples A and B.

Similarly, the characteristic amplitude and energy exponents for samples A and B (although the shapes of hysteresis loops are quite different in Fig. 5) are the same within the error bars in Table 3. This is not very surprising in the light of the results of [23] where it was observed, in similar $Ni_{49}Fe_{18}Ga_{27}Co_6$(at.%) single crystals, that in crystals with different γ-phase precipitates the AE distributions had almost the same exponents (see Table 3 in Ref. [23]). This can be related to the fact that the characteristic exponents are usually quite robust against of microscopic details, if the mechanism is the same. For instance, according to Ref. [32] the energy exponents for martensitic transformations with different martensite structures (from orthorhombic to tetragonal structures) vary only between 2.0 and 1.6. On the other hand, the most interesting difference observed in Ref. [23] was that the samples with different γ-precipitates had different asymmetry, defined by the following ratios: $\gamma_\varepsilon = \frac{\varepsilon_h - \varepsilon_c}{\varepsilon_c}$, $\gamma_\alpha = \frac{\alpha_h - \alpha_c}{\alpha_c}$ as well as $\mu = \frac{N_h - N_c}{N_c}$ and $\eta = \frac{E_{th} - E_{tc}}{E_{tc}}$ (see Table 5 in Ref. [23]), where the indexes h and c refer to heating and cooling). The other parameters in these ratios correspond to those shown in Table 3 above. Thus, the asymmetry parameters are more sensitive for the microscopic details of phase transformation and we will concentrate on them in the following discussions. In addition, it was shown in Ref. [33] that the above defined asymmetry parameters are interrelated: if γ_ε (and γ_α) are positive (called positive asymmetry [33]) then μ (and η) are negative. The advantage using μ (and η) instead of γ_ε (and γ_α) is that these are more accurate and can give definite sign of the asymmetry. Thus, from Table 3 we get that $\mu = 0.58$ and $\eta = 0.88$ as well as $\mu = -0.34$ and $\eta = -0.26$ for sample A and B, respectively, which means that the numbers of hits and the total AE energy during heating is larger for sample A (the transition is more "noisy" than for cooling), while the situation is just the reverse for sample B.

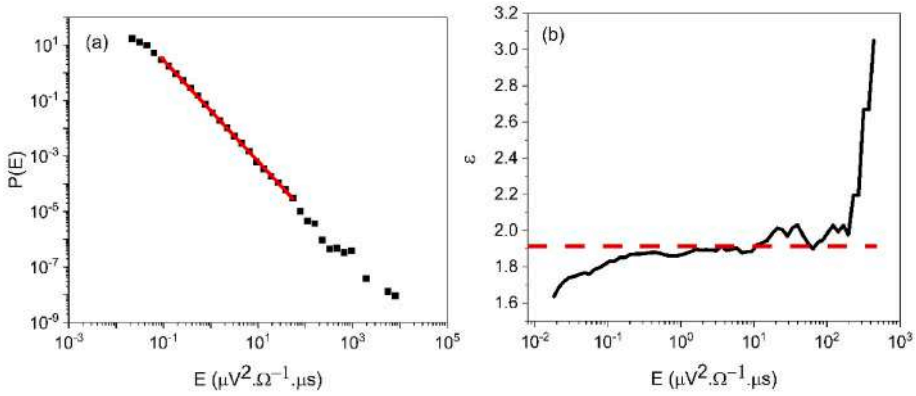

Fig. 13. Energy distribution functions for sample C; Log P versus log E, obtained from acoustic measurements during loading (a) at 383 K and the maximum likelihood fit (b) (the dashed line shows the value obtained from the fit, indicated by the straight line, in a): see also the text).

Table 5
Exponents of amplitude and energy distributions as well as the total numbers of hits and energies (N and E_t, respectively obtained during uploading and unloading at 383K. The error bars for the exponent ε and α are about ±0.1 and ± 0.3, respectively.

Sample	AE for uploading				AE for unloading			
	N	α	ε	E_t	N	α	ε	E_t
C	38346	3.0	1.8 (3)	2.07x 10^5	11518	2.8	1.8	2.77x 10^4

4.2. DSC and AE results for thermally induced and burst-like thermal recovery

We have seen in Chapters 3.2 and 3.3 that, depending on the temperature of compression, the mechanical loading can result in an incomplete or complete transformation to a stable martensite (see Fig. 8 and Table 4). From the results shown in Fig. 8a and Table 4, we can make a rough estimate of the volume fraction, $x = \frac{n_2}{n}$, of the stabilized martensite. Here n is the number of moles of the sample and n_1 and n_2 denotes the numbers of moles of twinned and detwinned martensites, respectively ($n = n_1 + n_2$). We can write for the quantities given in Table 4, that $q_{h1} = n_1 Q_{h1}$ and $q_h = nQ_h$ and q_{h3}=nQ_b. Here Q_{h1}, Q_h and Q_b denote the heat of transformations in units J/molK, and Q_{h1} and Q_h belong to the first peak in Fig. 8a during first heating as well as to the peak shown in Fig. 8b (from the first row of Table 4: $Q_h = 0.0670 J\frac{M}{m} = 256\frac{J}{molK}J$, where m=$1.6x10^{-5}$ kg and M is the molar volume M=0.0612 kg/mol). Q_b belongs to the complete burst-like transformation (from the last row of Table 4: Q_b=235J/molK). Thus,

$$\frac{q_{h1}}{q_h} = 0.79 = (1-x)\frac{Q_{h1}}{Q_h} \cong 1 - x \tag{3}$$

where we made the plausible assumption that $Q_{h1} \cong Q_h$, which leads to x = 0.21.

Another interesting result is obtained from the comparison of the heats and entropies of transformation for heating, during pure thermally induced transition as well as during thermal strain recovery after compression. We have two sets for comparison. For sample A (from Table 4) we get that, $\frac{Q_b}{Q_h} = 0.92$ and $\frac{S_b}{S_h} = \frac{s_b}{s_h} = 0.83$, while for sample C (from Table 2) $\frac{Q_b}{Q_h} = 1.03$ and $\frac{S_b}{S_h} = 0.88$ is obtained. The ratios of the above quantities, $\frac{Q_b s_h}{Q_h s_b}$, can also be compared with estimations based on the approximate relations for the peak temperatures of the transition, $T_p \cong \frac{Q}{S}$. This gives for the shift of the peak of thermal recovery, ΔT;

$$\frac{\Delta T}{T_{ph}} = \frac{T_{pb}}{T_{ph}} - 1 = \frac{Q_b s_h}{Q_h s_b} - 1 \tag{4}$$

Now, $\frac{\Delta T}{T_{ph}} = 0.12$, and $\frac{\Delta T}{T_{ph}} = 0.14$ for sample A and C, respectively from the measured ΔT values. On the other hand from (4), using $\frac{Q_b s_h}{Q_h s_b}$ from the above calculated ratios ($\frac{Q_b}{Q_h}$ and $\frac{S_b}{S_h} = \frac{s_b}{s_h}$), $\frac{\Delta T}{T_{ph}} = 0.11$ and $\frac{\Delta T}{T_{ph}} = 0.16$ are

Table 6
Power exponents in the scaling relations between the AE parameters E, A, and S.

	AE for loading		AE for unloading	
Power relation	log E versus log A	log S versus log A	log E versus log A	log S versus log A
Exponents	2.3 ± 0.3	1.5 ± 0.1	2.3 ± 0.2	1.4 ± 0.2

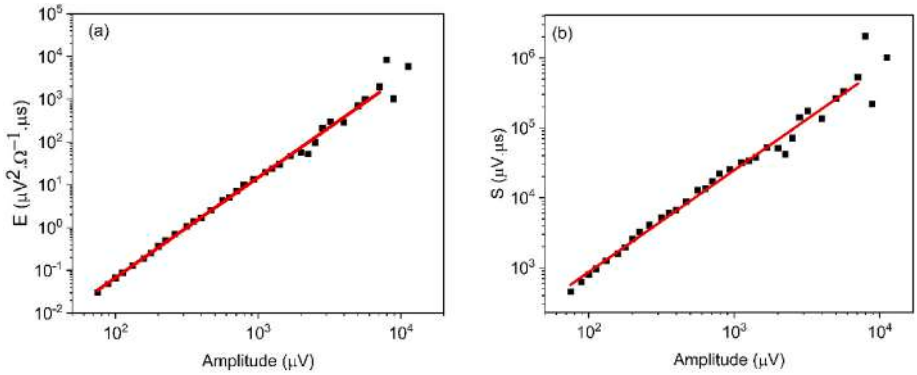

Fig. 14. Scaling relations between the AE parameters for sample C; (a) E versus A and (b) S versus A for loading.

obtained for sample *A* and *C*, respectively. It can be seen that the agreement, taking also into account the error bars, is very good.

From the above results we can also conclude that the main effect of the martensite stabilization is related to the decrease of the entropy by about 10%, while the change in the heat of transformation is much smaller. What should be the explanation for this decrease of entropy? The simplest explanation, based on the following qualitative arguments, fails: the (detwinned) martensite structure formed as a result of stabilization is less disordered, while the twinned (multivariant) structure is more disordered and thus, since for heating $S_h = S^A - S^M$ (and $S^A > S^M$), S_h is expected to increase. Similar conclusion can be drown from the relation between the transformation entropy and transformation strain according to the Landau theory, from which the $S \sim (\varepsilon^{tr})^2$ proportionality can be deduced [34], since ε^{tr} is larger for the stabilized martensite. This problem similarly arises for samples in which the martensite stabilization was achieved by SIM aging: in these cases a similar decrease of transformation entropy (by about 36-12%) was observed [35–37]. Thus, the explanation seems to be still open (see also the discussion in Ref. [35]) and more experimental (microscopic) and theoretical efforts are desired. For instance, as it was also mentioned in the introduction, in the burst-like recovery from the stabilized martensite, dislocations hindering the formation of the *DM/A* interphase boundaries and the nucleation barrier against retwinning can also play a role [2,3,14,38], and how these can be related (if are related at all) to the entropy change, is also an interesting question.

It can be seen, from the comparison of the DSC results (shown in Fig. 2b) well as the AE results (Fig. 3a and 3b), that the temperature range of the transitions on the DSC curves as well as on the changes of the cumulative energy or activity curves are in good agreement with each other. A similar conclusion can be drown from the comparison of Figs. 8a and Fig. 9 obtained during burst-like recovery: the temperatures of the maxima of the activity nicely agree with the DSC peak temperatures in Fig. 8a. It is worth noting that using the cumulative energy curve instead of the curves of cumulative number of AE events is more advantageous and provides a more clear representation of the sudden changes in the emitted AE (see also Fig. 10 in Ref. [39]). Furthermore, in contrast to Ref. [40], during heating we did not observe AE hits before the DSC A_s temperature (which was about 10% of the total numbers of hits and attributed to nucleation of austenite in Ref. [40]).

4.3. Stress-strain curves and AE results under compression along $[110]_A$ direction

In order to get a more detailed information on the relation between the acoustic emission and the course of the $\sigma \sim t$ curve we replotted Fig. 12a and b as shown in Figs. 15 and 16, where $\frac{d\sigma}{dt}$ *versus t* curves are shown instead of the $\sigma \sim t$ curves. Fig. 15 shows this derivative together with the AE activity, while Fig. 16 shows the cumulative number of energy, E_Σ, with the $\frac{d\sigma}{dt}$ *versus t* curves. It has to be noted that, from the constant strain rate $0.0017s^{-1}$ used, the time values on the horizontal axis can be easily converted to values of stain by $\varepsilon = 0.0017t$.

It can be seen in Figs. 12, 15 and 16 that during loading there is a quite remarkable acoustic emission already in the time domain where one would expect that only elastic deformation takes place. However, a close look of the $\frac{d\sigma}{dt}$ *versus t* curves, shows that this activity belongs to the deviation from the constant horizontal line, indicating a gradual change from the linear (elastic) regime. Thus, we identify this part as a fingerprint of the nucleation of *TM* martensite. This is accompanied with intensive acoustic emission with a definite jump in the E_Σ curve in the middle of this part (at about 30s), indicating the most intensive nucleation events with high AE energy. This result is similar to those obtained in Ref. [41], for AE measurements taken during compression test of Cu–Al–Ni single crystals: significant acoustic activity was observed before reaching the kink on the uploading stress-strain curve, which is usually considered as the martensite start stress.

Interestingly, there is a sharp decrease of the AE activity just at the first stress drop, after which the activity becomes low (about 10% of its value) and shows a local maximum at the second stress drop. The first and second stress drops can be attributed to the nucleation of detwinned, DM: after the first stress drop the stress is still large enough to maintain the nucleation of *TM* and at the next maximum the stress will be again high enough for the nucleation of *DM* again (see also [11]). It can be raised that the sharp decrease of the AE at the first stress drop is an experimental artifact: the sudden contraction of the sample could lead to loss of the contact with the AE sensor. We checked this by comparing three subsequent compression measurements at 383 K and, although some fine details (regarding the magnitudes and numbers of stress drops) were different, the above sharp decrease of the activity at the first stress drop was always present. Thus, we can conclude that the formation of *DM* is a sudden, fast process, during which the sample is "silent": if once the nucleation barrier for the formation of *DM* is overwhelmed, it can grow fast without significant elastic energy storage [11]. This is also reflected in the fact that during burst like recovery of DM, the thermal transition is very sharp, indicating that the stored elastic energy is close to zero [11,42].

For downloading, the first part, similarly to the first part of the $\frac{d\sigma}{dt} \sim t$ and $\sigma \sim t$ uploading curves in Fig. 15a and 16a, shows a moderate deviation of the stress versus time curve from the linear (elastic) regime and the observed acoustic activity in this region (at around 85s) presumably belongs to nucleation of small amount of *TM* (i.e. partial retwinning of *DM* [43]), with a small jumps in E_Σ (see the insert in Fig. 16b). It can also be seen, that at all stress jumps (at all maxima on the $\frac{d\sigma}{dt}$ versus t curve) there are local maxima on the AE activity curve. A closer look of the $\sigma \sim t$ downloading curve reveals some kinks at about 104 and 100 s too. We interpret at least the three well expressed stress jumps to sudden

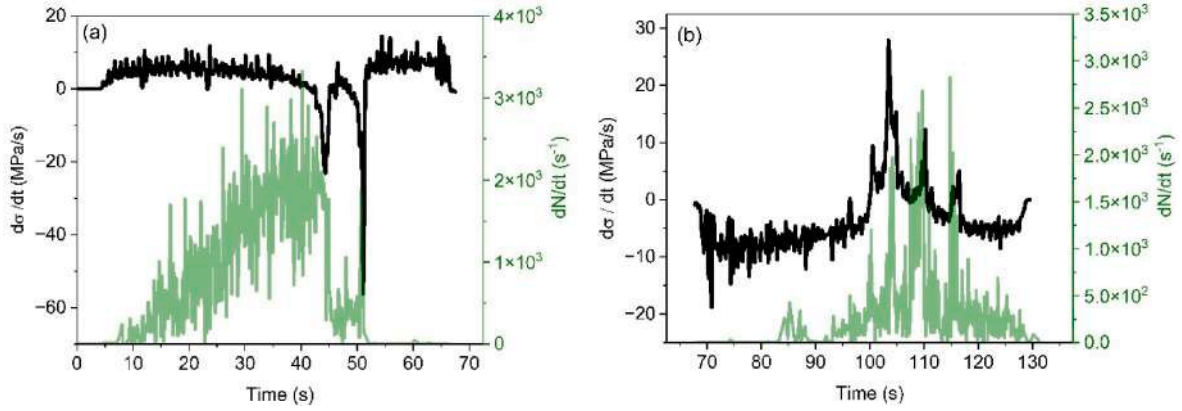

Fig. 15. Derivative of stress (black curve) and the acoustic activity (green curve): (a) uploading, (b) downloading for sample C.

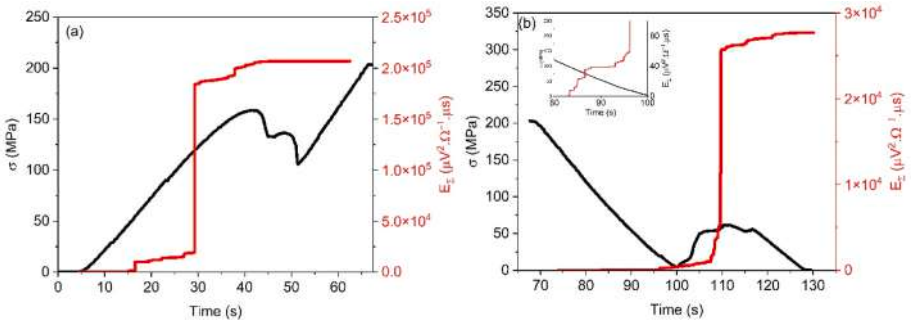

Fig. 16. Stress (black line) and cumulative energy versus time (red line): (a) uploading, (b) downloading for sample C (see also the text).

dissolution of the *DM* phase. In addition here the sharp jump in E_{Σ} appears at the second stress jump and this time moment coincides with the time when audible macroscopic click was heard. Finally, there is a continuously decreasing activity after the last stress jump (in the almost linear, austenitic, part in Fig. 16b). This can be attributed to dissolution of the remaining *TM* phase into austenite.

The above picture is in accordance with the literature about the problem of nucleation of that martensite modification which, although can be more stable if it is detwinned, do not have a common habit plane with the austenite [9,14,16,43]. Thus, the process starts first with nucleation of a self-accommodating (twinned) martensite (*TM*) and the nucleation of *DM* is more difficult and can happen at a higher stress level. Similarly, for the dissolution of *DM* a detwinning is required (leading to formation of *TM* as intermediate structural modification before the austenite can nucleate and grow). The large nucleation barrier for the formation of DM leads to stress drops on the uploading curves and the nucleation barrier for retwinning results in stress jumps on the downloading curves (with audible clicks). Indeed, it was illustrated in Ref. [11] that the temperature shift, ΔT, of the thermally induced DSC peak during burst-like recovery (as compared to the simple thermally induced heating peak) is a measure of the difference of the nucleation energy of *DM* and *TM*:

$$\Delta T \cong \frac{\Delta D}{-\Delta s} \tag{5}$$

where Δs is the entropy change during heating ($-\Delta s>0$). Since the nucleation energy, similarly to the dissipative energy, D, is positive for both directions, it was included in D [11,42]. From our data (see Table 2 for the transformation entropy for sample A, and Fig. 8 from which $\Delta T \cong 35K$), $\Delta D \cong 33$J/mol. It is worth to compare this result with half of the dissipative energy obtained from the area of the $\sigma\sim\varepsilon$ loops: 15J/mol: it can be seen that these are in the same order of magnitude (in getting eqn. (5) it was assumed [11] that the equilibrium temperature and the transformation entropy is the same for the temperature as well as compression induced phases). On the other hand, from the area of thermal hysteresis loop (where there was only the formation of *TM*), shown on Fig. 3a, $D/2 \cong 5.9$J/mol, which is indeed about one order of magnitude smaller.

Before summarizing, is it also worth mentioning that according to the results shown in Table 5, there is also an asymmetry here (similarly to the observed ones for the thermally induced AE): indeed $\mu = \frac{N_{unl}-N_l}{N_L} = -0.70$ and $\eta = \frac{E_{unl}-E_l}{E_l} = -0.86$, i.e. the loading branch is more "noisy" than the unloading one. It is interesting, that from acoustic investigations of degradation of Fe–Mn–Al–Ni shape memory single crystals, during cycling by compressive load along [001] direction, just an opposite asymmetry was observed [39], which points to sensitivity of this parameter on the microscopic details of the transformation.

We have seen that the acoustic emission measurements can provide quite interesting details about the anomalous stress induced (superelastic) behavior. Since the acoustic emission signals are related to sudden changes in the elastic energy [44], most probably such elastic energy changes during the nucleation events are the most important sources of acoustic emission in both directions, while the behaviour around the stress drops can be related to the nucleation/dissolution of the DM martensite. In addition we found that from the point of acoustic activity the loading and unloading processes are not equivalent: there is more AE emission events (and their cumulative energy is larger) for uploading than for downloading. This can also be related to the wisdom that the nucleation processes of the more stable martensite is more difficult [9–11,14,15]. Nevertheless the details around the stress drops are not fully clear yet and this calls for further measurements. For instance, from a thermodynamic analysis of such anomalous stress-strain curves during uploading, it was concluded in Ref. [11] that after the first stress drop (accompanied with the nucleation of DM martensite), depending on whether the fallen stress level is below the martensite start stress or not, either an elastic regime can be observed and re-nucleation of *TM* can start again, or the grows of *TM* takes place and the nucleation of *DM* happens again. This latter conclusion can be in agreement with our observations: e.g. for loading the first stress drop belongs to nucleation of *DM*, and after this the M1 *TM* grows further until the repeated nucleation of DM happens.

5. Conclusions

It is concluded from the two heating peaks in the DSC obtained after compression at 283K, that two martensite modifications (the twinned and detwinned ones) were present which transformed back at quite different temperatures. It was obtained that the transformation entropy of the burst-like transformation is smaller by about 10% than that of the thermally induced transformation.

The positions of the two sharp DSC peaks during burst-like recovery coincided very well with jumps on the curves of the cumulated acoustic energy, as well as with the maxima of the AE activity.

From simultaneous measurements of σ versus t and the AE versus time functions we obtained that

i) for uploading the AE activity gradually increased well below the maximum on the σ versus t function: this can be attributed to the nucleation of the (twinned) martensite. The two stress drops were attributed to the subsequent nucleation of the detwinned martensite from the twinned martensite. The sharp decrease of the AE activity just at the stress drops indicates that the formation of the detweinned modification is a sudden, fast process and can take place without significant elastic energy storage. This is supported by the fact that during burst like thermal recovery the width of the transition is very small i.e. the slope of the heating branch of this hysteresis curve is almost infinity.
ii) for downloading the first part shows a moderate deviation of the stress versus time curve from the linear (elastic) regime and the observed acoustic activity in this region presumably belongs to nucleation of small amount of the twinned martensits (i.e. to partial

retwinning). At all stress jumps there are local maxima on the AE activity curve. These were interpreted by sudden dissolution of the detwinned phase (retwinning). Finally, a continuously decreasing activity after the last stress jump (in the almost linear, austenitic, section) was attributed to dissolution of the remaining twinned phase into austenite.

In all cases the probability density distributions of parameters of AE avalanches followed the usual (power law) behaviour and e.g. the energy exponents were the same within the error bars for thermally or stress induced transformations in both directions. On the other hand, we found that from the acoustic activity during the loading and unloading processes were not equivalent: there are more AE emission events (and their cumulative energy is larger) for loading than for unloading. This can also be related to the wisdom that the nucleation processes of the more stable martensite is more difficult.

Author statement

We certify that all authors have seen and approved the final version of the manuscript being submitted. We warrant that the article is the authors' original work, hasn't received prior publication and isn't under consideration for publication elsewhere.

Declaration of competing interest

The authors declare that they have no known competing financial interests or personal relationships that could have appeared to influence the work reported in this paper.

Data availability

Data will be made available on request.

Acknowledgments

This work was supported by the National Research, Development and Innovation Office: NKFIH
PD131784 project.

References

[1] E.S. Machlin, M. Cohen, Transactions of AIME, J of Metals 3 (1951) 746, https://doi.org/10.1007/BF03397387.
[2] V.I. Nikolaev, S.I. Trepanov, P.N. Yakushev, V.M. Krymov, S.B. Kustov, Intermetallics, Burst-like shape recovery and caloric effects in Ni–Fe–Ga–Co single crystalline shape memory alloys, Intermetallics 119 (2020), 106709, https://doi.org/10.1016/j.intermet.2020.106709.
[3] G.A. Malygin, V.I. Nikolajev, V.M. Krymov, S.A. Pul'nev, S.I. Stepanov, Interfacial stresses and anomalous shape of pseudoelastic deformation curves in Ni49Fe18Ga27Co6 alloy crystals compressed along the [011] A Axis, Tech. Phys. 64 (2019) 819, https://doi.org/10.1134/S1063784219060124.
[4] V.I. Nikolajev, P.N. Yakushev, G.A. Malygin, A.I. Averkin, S.A. Pulnev, G.P. Zograf, S.P. Kustov, Y.I. Chumljakov, Influence of partial shape memory deformation on the burst character of its recovery in heated Ni–Fe–Ga–Co alloy crystals, Tech. Phys. Lett. 42 (2016) 399, https://doi.org/10.1134/S1063785016040209.
[5] S. Yang, T. Omori, C. Wang, Y. Liu, M. Nagasako, J. Ruan, H. Kainuma, K. Ishida, X. Liu, A jumping shape memory alloy under heat, Sci. Rep. 6 (2016), 21754, https://doi.org/10.1038/srep21754.
[6] D. Zhao, F. Xiao, Z. Nie, D. Cong, W. Sun, J. Liu. Burst-like superelasticity and elastocaloric effect in [011] oriented Ni50Fe19Ga27Co4 single crystals, Scripta Mater. 149 (2018), https://doi.org/10.1016/j.scriptamat.2018.01.029.
[7] C. Picornell, J. Pons, E. Cesari, Stress–temperature relationship in Cu–Al–Ni single crystals in compression mode, Mater. Sci. Eng. A378 (2004) 222, https://doi.org/10.1016/j.msea.2003.10.347.
[8] C. Picornell, J. Pons, E. Cesari, Stress-temperature relationship in compression mode in Cu-Al-Ni shape memory alloys, Mater. Trans. 45 (2004) 1679, https://doi.org/10.2320/matertrans.45.1679.
[9] P. Lazpita, E. Villa, F. Villa, V. Chernenko, Temperature dependent stress–strain behavior and martensite stabilization in magnetic shape memory Ni51.1Fe16.4Ga26.3Co6.2 single crystal, Metals 11 (2021) 920, https://doi.org/10.3390/met11060920.
[10] V.I. Nikolaev, P.N. Yakushev, G.A. Malygin, S.A. Pul'nev, Burst character of thermoelastic shape memory deformation in ferromagnetic Ni-Fe-Ga-Co alloy, Tech. Phys. Lett. 36 (2010) 914, https://doi.org/10.1134/S1063785010100123.
[11] D.L. Beke, S.M. Kamel, L. Daróczi, L.Z. Tóth, Thermodynamic analysis of anomalous shape of stress-strain curves for shape memory alloys, Materials 15 (2022) 9010, https://doi.org/10.3390/ma15249010.
[12] P. Sittner, V. Novak, N. Zárubová, Martensitic transformations in [001] CUAlZnMn single crystal, Acta Mater. 46 (1998) 1265–1281, https://doi.org/10.1016/S1359-6454(97)00323-6.
[13] Y. Liu, D. Favier, Stabilisation of martensite due to shear deformation via variant reorientation in polycrystalline NITI, Acta mater. (48) 2000, 3489, Acta Mater. 48 (2000) 3489–3499, https://doi.org/10.1016/S1359-6454(00)00129-4.
[14] C. Picornell, J. Pons, E. Cesari, Stabilisation of martensite by applying compressive stress in Cu-Al-Ni single crystals, Acta Mater. 49 (2001) 4221, https://doi.org/10.1016/S1359-6454(01)00308-1.
[15] R. Hamilton, C. Efstathiou, H. Sehitoglu, Y. Chumljakov, Thermal and stress-induced martensitic transformations in NiFeGa single crystals under tension and compression, Scripta Mater. 54 (2006) 465, https://doi.org/10.1016/j.scriptamat.2005.10.003.
[16] V. Novak, P. Sittner, N. Zárubová, Anisotropy of transformation characteristics of Cu-base shape memory alloys, Mater. Sci. Eng. A234–346 (1999) 414–417, https://doi.org/10.1016/S0921-5093(97)00175-5.
[17] Y. Imano, T. Omori, K. Oikawa, Y. Suttou, R. Kainuma, K. Ishida, Martensitic and magnetic transformations of Ni–Ga–Fe–Co ferromagnetic shape memory alloys, Mater. Sci. Eng. A. 438–440 (2006) 970, https://doi.org/10.1016/j.msea.2006.02.080.
[18] F. Xiao, M. Lin, J. Liu, X. Jin, Elastocaloric effect in Ni50Fe19Ga27Co4 single crystals, Acta Mater. 96 (2015) 292, https://doi.org/10.1016/j.actamat.2015.05.054.
[19] H. Morito, K. Oikawa, A. Fujita, F. Fukamichi, R. Kainuma, K. Ishida, Enhancement of magnetic-field-induced strain in Ni–Fe–Ga–Co Heusler alloy, Scripta Mater. 53 (2005) 1237, https://doi.org/10.1016/j.scriptamat.2005.08.009.
[20] E. Yu Panchenko, E.E. Timofeeva, L.P. Kyantseva, Y.I. Chumljakov, H. Maier, The effect of heat treatment on mechanisms of martensitic transformations in ferromagnetic single crystals, Russ. Phys. J. 53 (11) (2011) 1219–1222, https://doi.org/10.1007/s11182-011-9552-0.
[21] Y.I. Chumljakov, I.V. Kireeva, E.Y. Panchenko, V.A. Kirillov, E.E. Timofeeva, I. V. Kretinina, Y.N. Danilson, I. Karaman, H. Maier, E. Cesari, Thermoeastic martensitic transformations in single crystals with disperse particles, Russ. Phys. J. 54 (8) (2012) 937–950, https://doi.org/10.1007/s11182-011-9701-5.
[22] M.K. Bolgár, L. Daróczi, L.Z. Tóth, E.Y. Panchenko, Y.I. Chumlyakov, D.L. Beke, Effect of γ precipitates on thermal and acoustic noises emitted during austenite/martensite transformation in NiFeGaCo single crystals, J. Alloys Compd. 705 (2017) 840–848, https://doi.org/10.1016/j.jallcom.2017.02.167.
[23] M.K. Bolgár, L.Z. Tóth, S. Szabó, S. Gyöngyösi, L. Daróczi, E.Y. Panchenko, Y. I. Chumlyakov, D.L. Beke, Thermal and acoustic noises generated by austenite/martensite transformation in NiFeGaCo single crystals, J. Alloys Compd. 658 (2016) 29–35, https://doi.org/10.1016/j.jallcom.2015.10.173.
[24] A. Planes, J.L. Macqueron, J. Ortîn, Energy contributions in the martensitic transformation of shape-memory alloys, Phil. Mag. Lett. 57 (1988) 291–298, https://doi.org/10.1080/09500838808214716.
[25] D.L. Beke, L. Daróczi, T.Y. Elrasasi, Determination of elastic and dissipative energy contributions to martensitic phase transformation in shape memory alloys, in: F. Fernandes (Ed.), Shape Memory Alloys-Processing, Characterization and Applications, InTech, London, UK, 2013, p. 167, 978-953-51-1084-2.
[26] L.Z. Tóth, L. Daróczi, S. Szabó, D.L. Beke, Simultaneous investigation of thermal, acoustic, and magnetic emission during martensitic transformation in single-crystalline Ni2MnGa, Phys. Rev. B93 (2017), 144108, https://doi.org/10.1103/PhysRevB.93.144108.
[27] L. Carrillo, J. Ortín, Avalanches in the growth of stress-induced martensites, Phys. Rev. B 56 (1997), 11508, https://doi.org/10.1103/PhysRevB.56.11508.
[28] M. Le Blanc, L. Angheluta, K. Dahmen, N. Goldenfeld, Universal fluctuations and extreme statistics of avalanches near the depinning transition, Phys. Rev. E87 (2013), 022126, https://doi.org/10.1103/PhysRevE.87.022126.
[29] B. Casals, K.A. Dahmen, B. Gou, S. Rooke, E.K.H. Salje, The duration-energy-size enigma for acoustic emission, Sci. Rep. 11 (2021) 5590, https://doi.org/10.1038/s41598-021-84688-7.
[30] S.M. Kamel, N.M. Samy, L.Z. Tóth, L. Daróczi, D.L. Beke, Denouement of the energy-amplitude and size-amplitude enigma for acoustic-emission investigations of materials, Materials 15 (13) (2022) 4556, https://doi.org/10.3390/ma15134556.
[31] A. Clauset, C.R. Shalizi, M.E. Newman, Power-law distributions in empirical data, SIAM Rev. 51 (2009) 661–703. http://www.jstor.org/stable/25662336.
[32] A. Planes, L. Manosa, E. Vives, Acoustic emission in martensitic transformations, J. Alloys Compd. 577 (Supplement 1) (2013) S699–S704, https://doi.org/10.1016/j.jallcom.2011.10.082, 0.
[33] D.L. Beke, M.K. Bolgár, L.Z. Tóth, L. Daróczi, On the asymmetry of the forward and reverse martensitic transformations in shape memory alloys, J. Alloys Compd. 741 (2018) 106–115, https://doi.org/10.1016/j.jallcom.2017.11.271. JALCOM (2018.
[34] X. Ren, N. Miura, J. Zhang, K. Otsuka, K. Tanaka, M. Koiwa, T. Suzuki, Yu I. Chumljakov, M. Asai, A comparative study of elastic constans of Ti-Ni-based alloys prior to martensitic transformation, Mat. Sci. and Eng. A312 (2001) 196–206, https://doi.org/10.1016/S0921-5093(00)01876-1.
[35] N. Samy, L. Daróczi, L. Tóth, E.Y. Panchenko, Y.I. Chumlyakov, N. Surikov, D. L. Beke, Effect of stress-InducedMartensite stabilization on acoustic emission characteristics and the entropy of martensitic transformation in shape memory

Ni51Fe18Ga27Co4 single crystal, Metals 10 (2020) 534, https://doi.org/10.3390/met10040534.

[36] L.Z. Tóth, L. Daróczi, E. Panchenko, Y. Chumljakov, D.L. Beke, Acoustic emission characteristics and changethe transformation entropy after stress-induced martensite stabilization in shape memory Ni53Mn25Ga22 single crystal, Materials 13 (2020) 2174. https://doi:10.3390/ma13092174.

[37] M. Chandrasekaran, L. Cooreman, J. Van Humbeeck, L. Delaey, Martensitic transformation in Cu-Zn-Al: changes in transformation entropy due to post quench ageing in the β or martensitic condition, Scripta Metall. 23 (1989) 239–273, https://doi.org/10.1016/0036-9748(89)90418-3.

[38] F.C. Lovey, A. Amengual, V. Torra, M. Ahlers, On the origin of the intrinsic thermoelasticity associated with a single interface transformation in Cu-Zn-Al shape memory alloys, Phil. Mag. A 61 (1990) 159–165, https://doi.org/10.1080/01418619008235563.

[39] A. Weidner, A. Vinogradov, M. Vollmer, P. Krooβ, M.J. Kriegel, V. Klemm, Y. Chumljakov, T. Niendorf, H. Biermann, In situ characterization of the functional degradation of a [001] oriented Fe-Mn-Al-Ni single crystal under compression using acoustic emission measurements, Acta Mater. 220 (2021), 117333, https://doi.org/10.1016/j.actamat.2021.117333.

[40] J.M. Ball, K. Koumatos, H. Seiner, Nucleation of austenite in mechanically stabilized martensite by localized heating, J. Alloys Compd. 577S (2013) S37–S42. https://doi:10.1016/j.jallcom.2011.11.070.

[41] M. Landa, V. Novák, M. Balhácek, P. Sittner, Transformation processes in shape memory alloys based on monitoring acoustic emission activity, J. Acoust. Emiss. 20 (2002) 163–171. SSN 0730-0050, Copyright©2002 Acoustic Emission Group, Coden JACEDO.

[42] D.L. Beke, L. Daróczi, N.M. Samy, L.Z. Tóth, M.K. Bolgár, On the thermodynamic analysis of martensite stabilization treatments, Acta Mat 200 (2020) 490–501, https://doi.org/10.1016/j.actamat.2020.09.026.

[43] H. Seiner, P. Sedlák, M. Landa, Shape recovery mechanism observed in single crystals of Cu-Al-Ni shpe memory alloy, Ph. Transit. 81 (2008) 537–551, https://doi.org/10.1080/01411590801891616.

[44] P. Wollants, J.R. Roos, L. Delaey, Thermally- and stress-induced thermoelastic martensitic transformations in the reference frame of equilibrium thermodynamics, Prog. Mater. Sci. 32 (1993) 227–288, https://doi.org/10.1016/0079-6425(93)90005-6.